



HAL
open science

Gaussian Process NARX Model for Damage Detection in Composite Aircraft Structures

Samuel da Silva, Luis G. G. Villani, Marc Rébillat, Nazih Mechbal

► **To cite this version:**

Samuel da Silva, Luis G. G. Villani, Marc Rébillat, Nazih Mechbal. Gaussian Process NARX Model for Damage Detection in Composite Aircraft Structures. *Journal of Nondestructive Evaluation, Diagnostics and Prognostics of Engineering Systems*, 2021, 5 (1), pp.011007. 10.1115/1.4052956 . hal-03675467

HAL Id: hal-03675467

<https://hal.science/hal-03675467v1>

Submitted on 23 May 2022

HAL is a multi-disciplinary open access archive for the deposit and dissemination of scientific research documents, whether they are published or not. The documents may come from teaching and research institutions in France or abroad, or from public or private research centers.

L'archive ouverte pluridisciplinaire **HAL**, est destinée au dépôt et à la diffusion de documents scientifiques de niveau recherche, publiés ou non, émanant des établissements d'enseignement et de recherche français ou étrangers, des laboratoires publics ou privés.

Samuel da Silva

Associate Professor
Departamento de Engenharia Mecânica,
Faculdade de Engenharia de Ilha Solteira,
UNESP - Universidade Estadual Paulista,
Ilha Solteira, SP 15385-000, Brasil
e-mail: samuel.silva13@unesp.br

Luis G. G. Villani

Assistant Professor
Departamento de Engenharia Mecânica,
Centro Tecnológico,
UFES - Universidade Federal do Espírito Santo,
Vitória, Espírito Santo 13083-860, Brasil
e-mail: luis.villani@ufes.br

Marc Rébillat

Associate Professor
PIMM Laboratory, Arts et Métiers,
ENSAM/CNRS/CNAM,
Paris 75013, France
e-mail: marc.rebillat@ensam.eu

Nazih Mechbal

Full Professor
PIMM Laboratory,
Arts et Métiers,
ENSAM/CNRS/CNAM,
Paris 75013, France
e-mail: nazih.mechbal@ensam.eu

Gaussian Process NARX Model for Damage Detection in Composite Aircraft Structures

This article demonstrates the Gaussian process regression model's applicability combined with a nonlinear autoregressive exogenous (NARX) framework using experimental data measured with PZTs' patches bonded in a composite aeronautical structure for concerning a novel structural health monitoring (SHM) strategy. A stiffened carbon-epoxy plate regarding a healthy condition and simulated damage on the center of the bottom part of the stiffener is utilized. Comparing the performance in terms of simulation errors is made to observe if the identified models can represent and predict the waveform with confidence bounds considering the confounding effect produced by noise or possible temperature variations assuming a dataset preprocessed using principal component analysis. The results of the GP-NARX identified model have attested correct classification with a reduced number of false alarms, even with model uncertainties propagation regarding healthy and damaged conditions. [DOI: 10.1115/1.4052956]

Keywords: Gaussian process, NARX model, guided wave propagation, composite structures, nonlinear damage, stiffener debonding, propagation of uncertainties, damage classification, diagnostic decision support, diagnostic feature extraction, prognosis, structural engineering, testing methodologies, wave propagation modeling

1 Introduction

The Gaussian process (GP) regression models, also denominated as kriging metamodels, combined with nonlinear autoregressive with exogenous inputs (NARX) framework, are consolidated in the machine learning community, and numerous applications in nonlinear structural dynamics identification have been demonstrated [1–4]. Some advantages have explained this broad application in comparison with other nonlinear framework models. One of them is that the GP-NARX model is approximately nonparametric; i.e., there are fewer issues in choosing the order and structure of the nonlinear model to be used. When compared to the classical NARX models, GP-NARX does not necessitate the previous information or estimation about the nonlinear correlation between the regressors. However, the most significant benefit is related to the Bayesian framework of the GP-NARX formulation, where the confidence intervals are estimated naturally once an inference procedure identifies a covariance matrix of the estimation. Conversely, structural health monitoring (SHM) methods have found many issues to succeed when the structures operate in the nonlinear regime of motion and data uncertainties are manifested [5]. Among them, the confounding effects produced by the nonlinear phenomena and variability are practical deficiencies that can grow the number of false alarms [6].

Various procedures have been applied to make SHM robust in these situations, e. g., stochastic Volterra models [7], probabilistic tools [8], probabilistic model selection approaches [9], Bayesian approach based on a Markov-Chain Monte Carlo (MCMC) method [10], reliability assessment of measurement accuracy for FBG sensors [11], neural networks into deep learning procedures [12], and so on. Nonetheless, no robust application of the

GP-NARX models for SHM purposes is known by the authors. The advantage of this approach provides information about the model uncertainties in the output estimation. This feature of GP-NARX models provides exploring the statistical confidence bands estimated by the metamodel in a robust SHM scheme with some benefits contrasting with the other current methods. One of them is that in an SHM's hierarchy, e. g., quantification and prognosis, it is also imperative to hold a mathematical model based on past data to interrogate the existence and evolution of damage. These models demand to combine knowledge about the damage behavior in its dynamics to obtain information about the monitored structure. Unfortunately, numerical models, for example, using finite element models, require much time and have a high cost for a real-time SHM system [13]. Another restriction is that the damage evolution, mainly in composite structures, usually is troublesome to be modeled in a real-world application due to a range of effects that can appear coincidentally with particular confounding aspects, like noise, uncertainties, and temperature fluctuations, including nonstationarity, nonlinear wave interactions, etc. The application of GP-NARX models aims to overcome these several shortcomings. Creating an interval of confidence through the GP-NARX model is plausible to accommodate these changes occasioned by noise or temperature fluctuations.

The use of autoregressive family models of Lamb waves was already broadly used in the literature for SHM in composites structures [13–15]. However, the benefits of GP-NARX to earn a better prediction model of composite structures and, mainly, to process the uncertainties regularly are not commonly practiced for SHM. For the authors' knowledge, this is the first article to assume this more complicated situation. Thus, a challenging application to demonstrate these issues is discussed in the present article concerning an aeronautical stiffened carbon-epoxy plate with a network of bonded PZTs acting as actuators and sensors to propagate Lamb waves [16]. The effect of reflections and wave interactions caused

by the stiffer and damage is an actual challenge to be captured by a robust model. A set of GP-NARX models is obtained to identify the model-predicted output (MPO) with infinite step-ahead assuming temperature effects and different outlines of healthy and damaged states, where there is a real debonding in the center of the plate. In all cases, the uncertainties are propagated by MC simulations in the GP-NARX estimated models' feedback to make the results realistic and consider the uncertainties related to the estimated model [3]. Two damage indices are tested, one utilizing the prediction errors and another one counting the outliers outside of the uncertainty boundaries provided by the GP-NARX metamodel with MC simulations in healthy conditions, assuming several variations of temperature to observe the robustness of the procedure. Principal component analysis (PCA) is already broadly used to extract features for damage detection with insensitivity to temperature effects [17,18]. Here, the central idea is to perform a previous condensation of the wave signals assuming a known gradient of temperatures using PCA to train the healthy GP-NARX models and accommodate this change in the variance the metamodel.

This article is organized as follows. A survival and overview of GP-NARX models are primarily presented to explain and adapt its characteristics to SHM. Next, an experimental setup case involving a stiffened carbon-epoxy coupon and the robust identification is handled to capture the dynamics using the measured data. A damage assessment procedure using the prediction errors is examined, assuming the fluctuations caused by temperature effects. Based on this first result, an enhanced version of the Kriging metamodel is obtained by applying a principal component analysis by analyzing a different set of temperatures in the procedure's training step. With this novelty proposal, another damage index is implemented concerning the model predictions' outliers. Finally, the conclusions are addressed, and future directions are recommended.

2 An Overview of Model-Predicted Output by GP-NARX

In this formulation, it is assumed that the output signal $y_i \in \mathbb{R}$ measured by a PZT patch can be described by a nonlinear regression [19]:

$$y_i = f(\mathbf{x}_i) + \varepsilon_i^y, \quad i = 1, 2, \dots, N \text{ instants} \quad (1)$$

where $f(\cdot)$ is an unknown nonlinear function, $\mathbf{x}_i \in \mathbb{R}^D$ is the model's input, and ε_i^y is a zero mean Gaussian noise defined by

$$\varepsilon_i^y \sim \mathcal{N}(\varepsilon_i^y | 0, \sigma_y^2) \quad (2)$$

where σ_y^2 is the variance of the process. Considering the NARX structure to represent the output signal y_i , the model's input \mathbf{x}_i is formed by the regressors of the excitation and output signals

$$\mathbf{x}_i = [y_{i-1} \quad \dots \quad y_{i-n_y} \quad u_i \quad \dots \quad u_{i-n_u+1}] \quad (3)$$

where $u_i \in \mathbb{R}$ is an excitation signal, n_y , and n_u are the number of regressors in the output and excitation signals, respectively. Thus, a training dataset \mathcal{D} is assumed for different time-instants

$$\mathcal{D} = (\mathbf{x}_i, y_i)_{i=1}^N \equiv (\mathcal{X}, \mathcal{Y}) \quad (4)$$

where $\mathcal{X} \in \mathbb{R}^{N \times D}$ is the regression matrix, and $\mathcal{Y} \in \mathbb{R}^N$ is the output vector.

Considering the GP-NARX model structure, the nonlinear function $f(\cdot)$ is assumed as a zero mean multivariate Gaussian prior [20]:

$$\mathbf{f} = f(\mathcal{X}) \sim \mathcal{N}(\mathbf{f} | 0, \mathcal{K}) \quad (5)$$

where $\mathcal{K} \in \mathbb{R}^{N \times N}$ is the covariance matrix with $\mathcal{K}_{ij} = k(\mathbf{x}_i, \mathbf{x}_j)$, and $k(\cdot, \cdot)$ is the *kernel* function, also named by covariance function. The zero mean is assumed for simplicity, considering the flexibility

of the GP-NARX model [19].

In this sense, the output is calculated considering a Bayesian inference over functions, using the multivariate Gaussian prior, the training data set, and the covariance function, represented by the kernel function. The kernel function can assume different forms depending on the problem at hand, and it may significantly influence the system's dynamical behavior. In this study, an exponential and isotropic kernel is used:

$$k(\mathbf{x}_i, \mathbf{x}_j) = \exp \left[-\frac{1}{2} w^2 \sum_{d=1}^D |x_{id} - x_{jd}| \right] \quad (6)$$

where w^2 is the hyperparameter that drives the model's covariance function. This choice is due to the smooth trend observed in the output signals. Considering a Gaussian likelihood

$$\mu(\mathcal{Y} | \mathbf{f}) = \mathcal{N}(\mathcal{Y} | \mathbf{f}, \sigma_y^2 \mathcal{I}) \quad (7)$$

where $\mathcal{I} \in \mathbb{R}^{N \times N}$ is the identity matrix, and the Bayesian inference is used in the calculation of the unknown output as a consequence of a new input \mathbf{x}_*

$$p(f_* | \mathcal{Y}, \mathcal{X}, \mathbf{x}_*) = \mathcal{N}(f_* | \mu_*, \sigma_*^2) \quad (8)$$

$$\mu_* = \mathbf{k}_{*N} (\mathcal{K} + \sigma_y^2 \mathcal{I})^{-1} \mathcal{Y} \quad (9)$$

$$\sigma_*^2 = k_{**} - \mathbf{k}_{*N} (\mathcal{K} + \sigma_y^2 \mathcal{I})^{-1} \mathbf{k}_{N*} \quad (10)$$

where $\mathbf{k}_{*N} = [k(\mathbf{x}_*, \mathbf{x}_1), \dots, k(\mathbf{x}_*, \mathbf{x}_N)]$, $\mathbf{k}_{N*} = \mathbf{k}_{*N}^T$, $k_{**} = k(\mathbf{x}_*, \mathbf{x}_*)$. A predictive distribution of y_* is similar to f_* , but with the addition of the variance σ_y^2 . The hyperparameters $\Theta = [\sigma_y^2, w^2]^T$ are determined through an optimization procedure considering the likelihood of the log-marginal and a set of training data:

$$\log \mu(\mathcal{Y} | \mathcal{X}, \Theta) = -\frac{1}{2} \log |\mathcal{K} + \sigma_y^2 \mathcal{I}| - \frac{1}{2} \mathcal{Y}^T (\mathcal{K} + \sigma_y^2 \mathcal{I})^{-1} \mathcal{Y} - \frac{N}{2} \log(2\pi) \quad (11)$$

An extensive sensitivity is observed depending on the training data, the kernel function assumed, and the regression order. In addition, considering infinity step-ahead prediction, the next step prediction is a function of the measured excitation signal and the output previously estimated by the model. However, the output of the model in each time instant has a Gaussian distribution defined by a mean $\mu(y_i)$ and a variance of $\sigma^2(y_i)$. So, Monte Carlo simulations are used to back-propagate the model output uncertainties into the model, considering all the uncertainties in the response estimation process [3]. Finally, the GP-NARX estimated can be used concomitantly with MC simulations to predict the structure's expected output.

3 Experimental Setup Case: A Stiffened Carbon-Epoxy Plate

Figure 1 shows a monolithic carbon-epoxy composite stiffened plate with 400 mm \times 300 mm of width and height, respectively, with a stiffener and a multilayered structure consisting of 4-ply oriented along [0 deg/45 deg/-45 deg/0 deg]. A network of six PZTs elements has been bonded to the stiffened plate's surface at specific positions, as shown in Fig. 1. In this arrangement, each PZT is used sequentially as an actuator, excited with a five cycles *burst* signal with a central frequency of 200 kHz and amplitude of 10 V. This choice of the signal is made based on the previous study to find the best parameter to excite the plate adequately to observe all dynamics effects and the possible interaction between

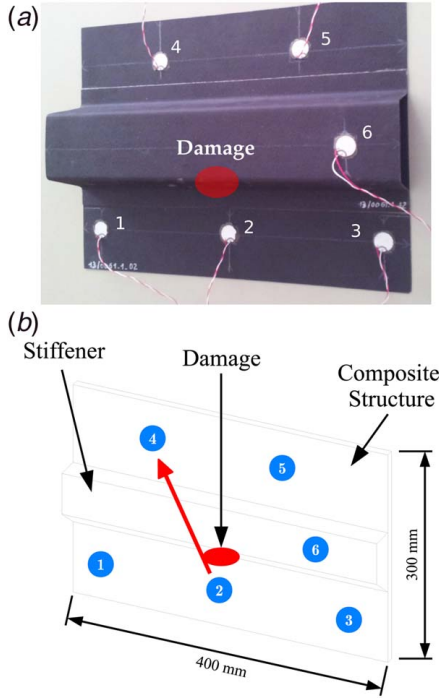


Fig. 1 Experimental setup with the 6 PZTs adapted from Mechbal and Rébillat [16]: (a) view of the stiffened carbon-epoxy plate and (b) damage position and example of a wave path

the stiffeners and the existence of damage [16]. Generally speaking, a narrow band frequency excitation is preferred to avoid dispersion-related undesirable effects. However, we also have to deal with the finite nature of the specimen under study leading to boundary reflections. To limit the impact of those reflections, the input signal should be band limited. Consequently, five cycles of tone bursts windowed by a cosine or Hanning window appear as the kind of signals that best suits both aspects and the choice that has been made here. In contrast, the other PZTs are used as sensors, recording simultaneously the PZTs outputs for 1000 data points sampled at 1 MHz. A combination of 36 paths can be utilized to calculate damage-sensitive index features with several operating conditions.

All experiments were conducted inside of a temperature chamber to control the environmental variability, analyzing six different

temperatures of 0 °C, 15 °C, 30 °C, 45 °C, 60 °C, and 75 °C in both healthy and damaged situations. In each state, ten repetitions were realized to insert some variability in the experimental realizations. Each time histories are normalized to have zero mean and standard deviation of one. Delamination is simulated in the stiffener's foot by adding a small Teflon insert before the curing process. This prevents bonding the stiffener and the plate at the insert position, as discussed in Ref. [16].

3.1 Identification of Guided Wave Propagation Using GP-NARX Models. The first step is to determine the number of regressors n_y and n_u necessary for each path. A simple metric can be established to help decide this based on the computation of the following expression of fit (%):

$$\text{Fit}(n_y, n_u) = 100 \left(1 - \frac{|y(n_y, n_u) - y_{exp}|}{|y_{exp} - \bar{y}_{exp}|} \right) \quad (12)$$

where y is the mean of model-predicted output by GP-NARX in function of order-lag n_y and n_u , y_{exp} is the experimental output, and \bar{y}_{exp} is the mean of the experimental output. With a focus in model-predicted output for the PZT path 2–4, illustrated in Fig. 2, is observed that $n_y = 120$ and $n_u = 100$ warrant >85% of fit. All paths warrant a similar fit for these lag-orders.

To illustrate the procedure of identification, only a reference temperature of 30 °C was considered, with regression order of $n_y = 120$ and $n_u = 100$. The mean of the input and output signals of the ten training healthy condition data was employed to fit a GP-NARX metamodel. An exponential covariance kernel was chosen, and the model's hyperparameters were estimated using a gradient optimization method. Figure 3 presents the model-predicted output for GP-NARX healthy model for some PZTs paths comparing the mean of the metamodel obtained with an experimental observation measured in a randomly testing condition, where the confidence bounds were computed with 3σ for each sample. The results manifest that the uncertain confidence bands can well accommodate the experimental data even in the wave reflections region. A considerable uncertainty before the first wave packet's arrival is discerned due to the wave propagation delay among the excitation and output measured, generating an uncertain zone.

A backpropagation of uncertainties demands to be performed to consider all the uncertainties associated with the model, as suggested by Ref. [3]. Thus, the output y_i was sampled from a Gaussian distribution using the estimated mean and variance computed through the GP-NARX model in each instant. A Monte Carlo

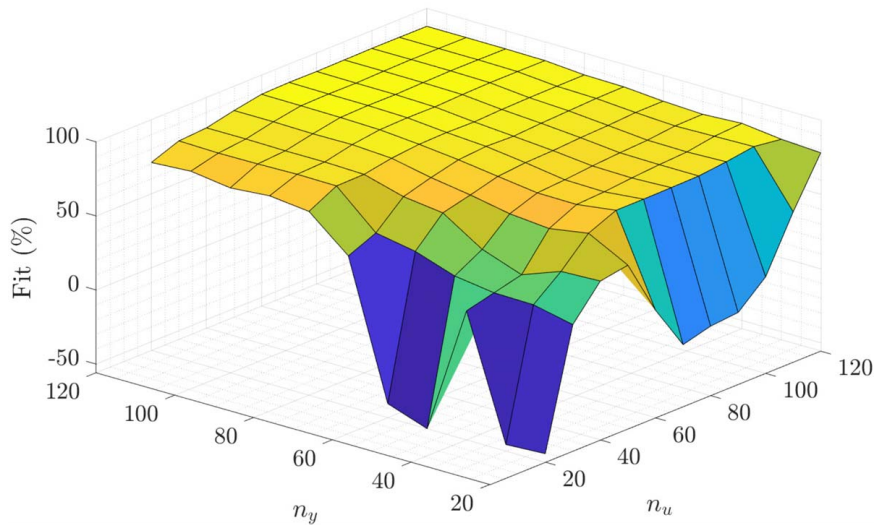


Fig. 2 Order selection with focus in model-predicted output for the PZT path 2–4 at 30 °C

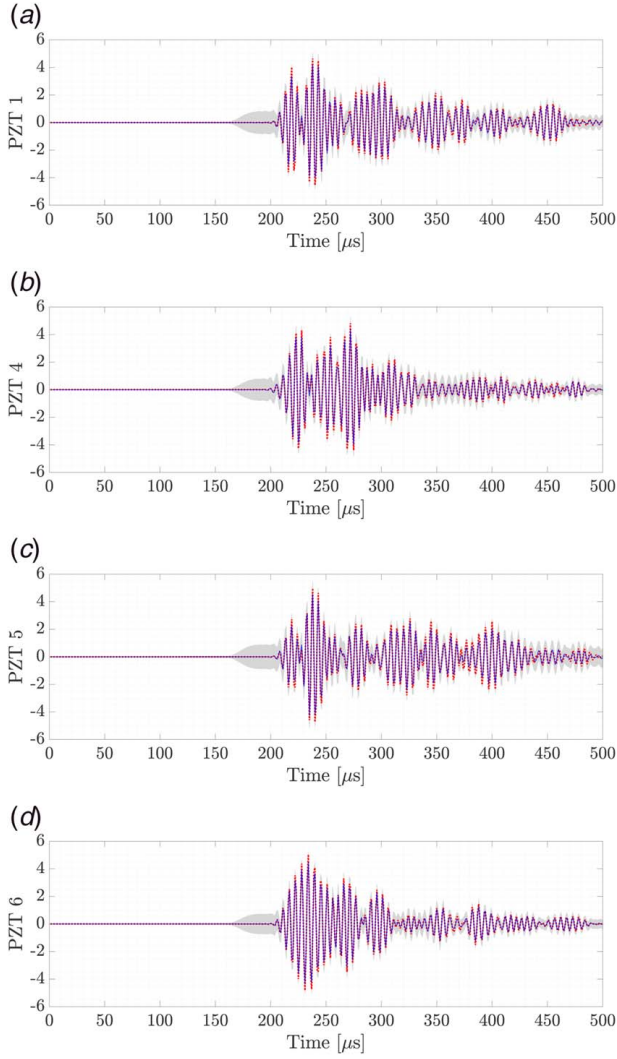


Fig. 3 Model-predicted output for GP-NARX healthy model of different PZTs paths, where —, GP-NARX metamodel; ···, experimental observation; ■, 3σ uncertainty bounds: (a) path 2 → 1 with fit of 85.7%, (b) path 2 → 4 with fit of 86.6%, (c) path 2 → 5 with fit of 82.2%, and (d) path 2 → 6 with fit of 88.2%

simulation with 100 realizations was run. Now a more pragmatic interval of uncertainty is captured, as shown in Fig. 4, where the mean and variance of the Monte Carlo realizations are used to compute the 3σ confidence bounds. The increase of the confidence bands is a direct consequence of the uncertainties backpropagation, reducing the efficacy of the prediction, mainly close to the reflections caused by the stiffener (see Figs. 4(b)–4(d)), where the confidence interval is more significant. As addressed in the following sections, this is a confounding factor when assuming temperature effect and damage condition that can render a false alarm if we use simple damage feature indices.

3.2 Damage Assessment Using GP-NARX Model. A simple damage index DI can be computed by

$$DI = \frac{\|y - y_{exp}\|}{y_{exp} - \bar{y}_{exp}} \quad (13)$$

where y is the mean of healthy MPO by GP-NARX framework, y_{exp} is the experimental output in unknown condition, and \bar{y}_{exp} is the mean of the experimental output.

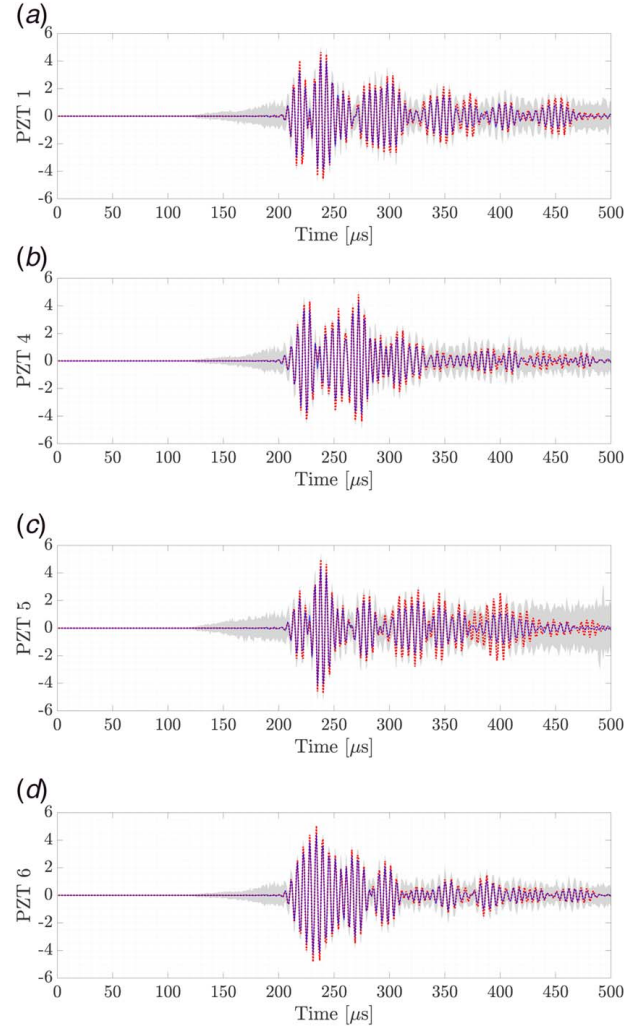


Fig. 4 Monte Carlo prediction for GP-NARX healthy model of different paths, where —, mean of the GP-NARX metamodel; ···, experimental observation; ■, 3σ uncertainty bounds: (a) path 2 → 1, (b) path 2 → 4, (c) path 2 → 5, and (d) path 2 → 6

Figure 5 illustrates the box plot to observe the median, quartiles, and outliers of the distributions of this DI in Eq. (13) for some paths considering PZT 2 as an actuator for healthy and damaged states by propagating uncertainties into predictions of the GP-NARX model using Monte Carlo simulation with 100 runs. In each case, ten experimental tests were performed to inject some intrinsic variability after propagated by Monte Carlo simulations using the mean and variance estimated by the GP-NARX model. It is also worth observing that the GP-NARX model is obtained by randomly choosing only one of the time-series in the healthy states in the ten realizations. Thus, the reference model is representative of all situations in a healthy condition.

Consequently, all these situations are correctly assigned to the actual structural condition showing that this DI is sensitive to the presence of damage for all paths even by backpropagation of the uncertainties performed in the MPO of the GP-NARX model. Any simple classifier can indeed separate the two states. A more significant difference between the damage indices between the two clusters (healthy and damage conditions) is observed looking at the pathway 2–4, once for this scenario resembles the direction where the damage is located. Thus, only this path will be illustrated in the subsequent analyses without loss of generalization and simplicity. Figure 6 proves the performance of this damage index DI using the receiver operating characteristics (ROC) curve for the path 2–4.

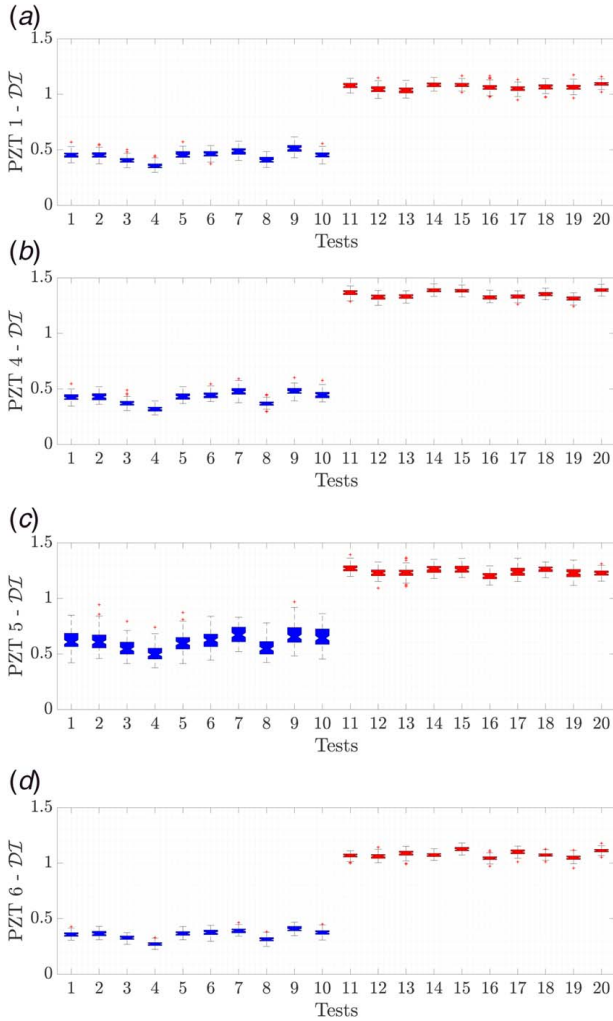


Fig. 5 Box plot of the DI considering some paths by propagating uncertainties using Monte Carlo simulations with 100 runs: ■ healthy versus ■: (a) path 2 → 1, (b) path 2 → 4, (c) path 2 → 5, and (d) path 2 → 6

3.3 Effects of Temperature Changes. Unfortunately, the last scenario is unreal because it was assumed only a trained GP-NARX model analyzing the temperature reference of 30 °C. If it is measured the same situations regarding a range of six different temperature's changes defined by 0 °C, 15 °C, 30 °C, 45 °C, 60 °C, and 75 °C, a phase shift occurs, as shown in Fig. 7 considering the PZT's path 2–4 and the undamaged situation. The temperature

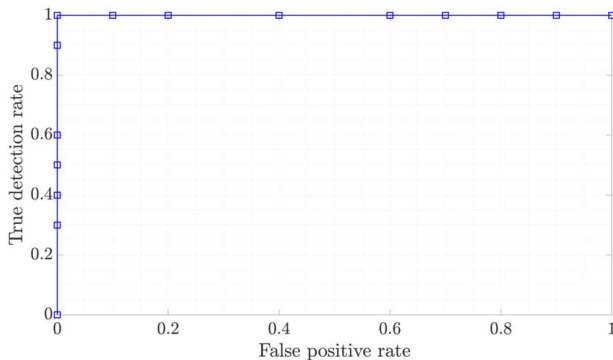


Fig. 6 ROC curve of the mean of DI for the path 2 → 4

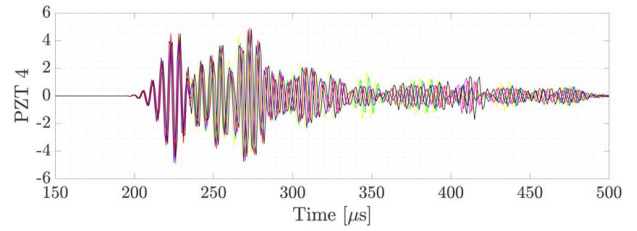


Fig. 7 Temperature effect in one realization of healthy state signals: 0 °C, 15 °C, 30 °C, 45 °C, 60 °C, and 75 °C

effects cause some changes in the phase due to the coupling piezo-electric effect. Typically, in the literature, several approaches can be applied to compensate using some classical procedures. It is expected a mistaken classification if there is no attention to the temperature effect in the analysis. This problem is worse yet when assuming the backpropagation of the uncertainties using the mean and the variance estimative of the reference GP-NARX model in the computation of the damage indices attempting a robust classification.

Figure 8 illustrates 120 different conditions in two groups of healthy and damaged situations, assuming temperature changes for the path 2–4. The reference state is again chosen randomly, assuming the temperature of 30 °C, dataset in magenta in Fig. 8. In each case, the states are feed by propagating uncertainties through Monte Carlo simulation with 100 runs. This damage index computed using the GP-NARX model without counting the temperature variations fails to recognize the actual states with robustness, as shown in Fig. 8. Figure 9 confirms these results by analyzing the ROC curve to detect damage against the reference condition regarding the mean of the DI in each condition. There is an overlap between the healthy and damaged boxplot, making it more difficult to distinguish the structural state when temperature changes and uncertainties are assumed.

Of course, if a range of more training data assuming the temperature changes is taken in a supervised mode, the classification is more suitable. However, the damage index is shown in Eq. (13) uses the difference between the mean of one reference GP-NARX model in a healthy condition; even if there is a possible difference among them, if it is inside the limit confidence interval indicates that there is any significant alteration to be correlated with damage. One point here should be to use multiple models. However, how it will be discussed next section, a more simple form can be used to detect the damage in this scenario, with a robust classifier, if the variance of the GP-NARX is applied combined with principal component (PC) compression of signals to identify virtual GP-NARX models robust to all temperature conditions in the healthy state. The key

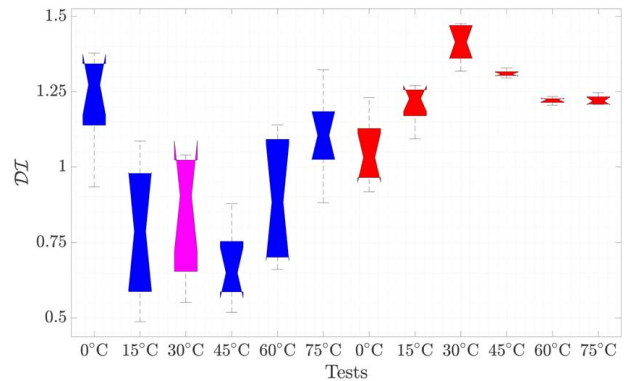


Fig. 8 BoxPlot of the DI for ■ healthy versus ■ damaged assuming temperature changes for the PZT path 2–4. The reference model is identified using the temperature of 30 °C using the training data described by ■.

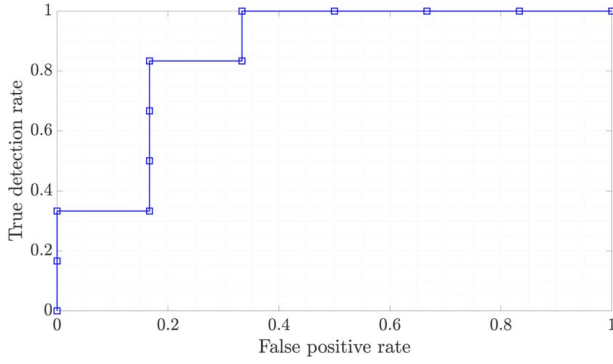


Fig. 9 ROC curve considering temperature effect for the path 2 → 4

idea is applying an uncomplicated metric to count the outliers, the number of points outside the limit of the uncertainty interval.

4 Robust Damage Detection Using Kriging Metamodel

Temperature compensation is typically used to mitigate the influence of temperature variations in the computation of the damage indices features for SHM [21]. In the present article, the temperature is modeled in the reference GP-NARX in the training step using a data fusion to generate a virtual signal to represent all variations of temperature examined. Thus, a new MPO healthy GP-NARX model assumes the PCs of the dataset with this range of temperature variations.

A matrix \mathbf{Y}_i of the time-series corresponding PZTs output to m temperature variations and sampled at l time interval is formed at a given temperature i

$$\mathbf{Y}_i = [y_1(i) \quad y_2(i) \quad \cdots \quad y_m(i)]^T \quad (14)$$

A $m \times m$ covariance matrix $\mathbf{\Omega}$ among temperature variations summed over all time samples is computed by [22]:

$$\mathbf{\Omega} = \sum_{i=1}^l \mathbf{Y}_i \mathbf{Y}_i^T \quad (15)$$

If an eigenvalue problem is calculated using the covariance matrix, the eigenvalue α_i and the eigenvector \mathbf{v}_i can be used to reduce the m – dimensional vector into a d – dimensional vector with $d < m$. Thus, a virtual signal z could be used by summing the contributions of each eigenvector by

$$z_i = [\mathbf{v}_1 \quad \cdots \quad \mathbf{v}_d]^T \mathbf{Y}_i \quad (16)$$

Figure 10 illustrates the PC of the dataset, assuming again the PZT patch 2 → 4 for the covariance of the output signal. $d = 4$ principal

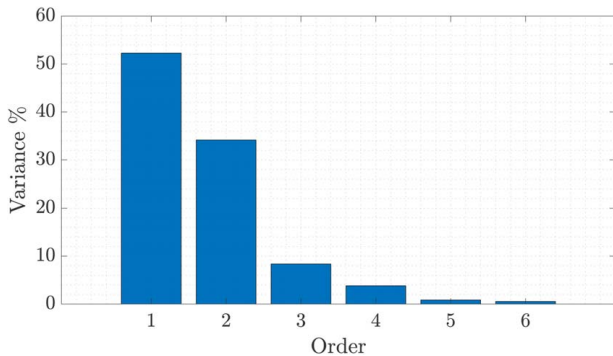


Fig. 10 PCA of the output covariance matrix for the PZT path 2 → 4

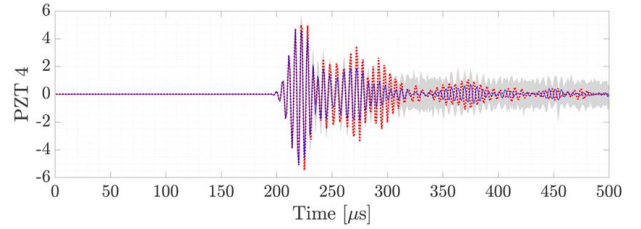


Fig. 11 Monte Carlo prediction for GP-NARX model obtained by the virtual signal for healthy condition where – is mean of the GP-NARX metamodel, ... is experimental observation in a randomly temperature test, and ■ is 3σ uncertainty bounds

components are utilized, and the virtual signal applied for training the GP-NARX is assumed by summing all four components.

The same regressor order and parameters used before are repeated to compute the reference GP-NARX model using the virtual signal. Figure 11 illustrates the Monte Carlo simulations with 100 runs compared to an experimental observation chosen randomly. It is worth noting that all potential temperature variations are now adequately contained inside the confidence interval of this new model. As pointed out earlier, the region of reflections continues to be the more uncertain region of wave propagation.

Once this reference model is suitable to MPO in the healthy state, the central idea to propose here is to count the number of outliers, named here by γ , that is outside of the confidence interval estimated by the variance of GP-NARX. This is a more efficient way to distinguish with robustness against the reference some potential damage state because the confidence interval contained the uncertainties and possible alterations associated with temperature fluctuations if the training step is adequate. If the number of outliers is increased, an alert of damage may be triggered. Figure 12 exhibits the box plot of this index using the outliers for the testing path, demonstrating that a better performance is reached.

Figure 13 presents the ROC curve of the number of outliers γ to reinforce a more reliable performance of this damage-sensitive index concerning the outliers outside the uncertainty bound limits. Minor performance may happen in a real scenario once typically simultaneous damages appear. A ROC curve with less area is expected; however, the different paths tested can help decide the structural state if multiple GP-NARX models are estimated for all PZTs. The results found in the present article proves an outstanding use of this Bayesian model for SHM or dynamic analysis purpose.

It is worth remarking that the feature used in this article is extracted from a time-domain procedure involving the variance of the prediction error computed by the GP-NARX model. Combining other elements calculated in the frequency domain can include additional information to understand the damage state better. However,

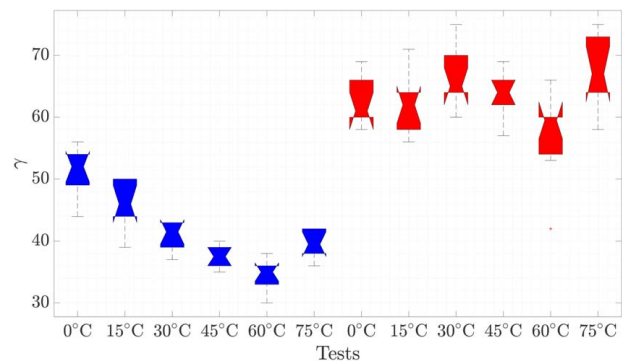


Fig. 12 Box plot of the index γ (outliers) for healthy versus damaged assuming temperature changes to the PZT path 2–4. The reference model is identified using a virtual signal compressed by PC.

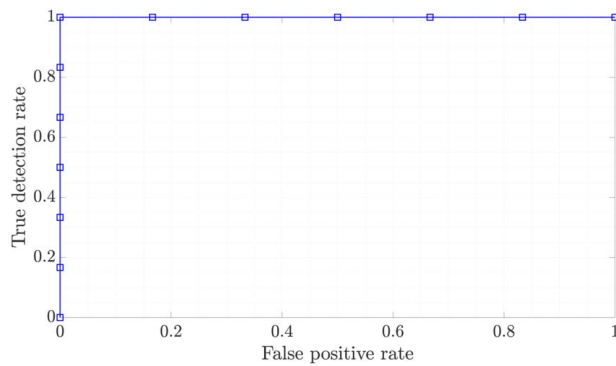


Fig. 13 ROC of curve of the damage index γ considering temperature effect

it is essential to assume the low information possible without a considerable post-processing to evaluate the structural condition.

5 Conclusions

This article demonstrated the practical utilization of a GP-NARX framework for modeling wave propagation in composite coupons with stiffeners. An MPO with an infinite horizon is obtained and used to simulate the composite structure's operation, assuming healthy conditions. A combined Monte Carlo simulation using the estimated mean and variance in each time sample using a network of the PZTs bounds enables us to hold comprehensive information about the structural state.

Besides the efficiency of modeling aiming simulation purposes, structural health monitoring is also discussed, adopting a damage index involving prediction errors. Some tests are performed assuming a damaged condition caused by debonding, and adequate performance to classify the structural state is reached. However, the temperature influence can generate fluctuations, and the method can be improved by assuming a broad range of temperature changes in the training step. The major weakness of manipulating only some temperatures to train a single GP-NARX model for testing other temperature conditions is that this type of model cannot extrapolate situations different from those that are not trained. So, we hold a remarkable ability to train in various temperatures and test some cases inside this array of temperatures. However, if we decide to treat temperatures outside this scope, the model decreases the performance, and the uncertainty intervals could expand. In that sense, a virtual sensing signal compressed by principal components of a matrix of temperature variations is used to train a new GP-NARX surrogate model that enables the modeling in the healthy state, including the temperature changes and the other uncertainties not associated with damage. A more assertive classification is obtained with this model. Estimating the variance of a GP-NARX model is also beneficial for introducing a new and straightforward damage index by counting the number of outliers outside the uncertain-bound limits. The results have shown that simple classifiers and hypothesis tests could be used to detect the structural state's reliability.

This method's significant benefit is to offer an MPO estimate of the wave propagation in the healthy state and a robust detector to uncertainties and temperature effect using the natural variance estimated by the GP-NARX model. Another meaningful advantage is the possibility of quickly modeling, aiming to simulate any complex geometry in any physical system using a low-cost and black-box method. If the stiffener is altered or the position of the damage is modified, the effects in the signal networks will be different. Consequently, for the success of this approach, it is necessary to identify an adequate GP-NARX prediction model. This is an advantage of this class of identification model because this includes information about the model's uncertainty. In addition, the Bayesian

framework allows direct adaptation of the baseline model to different conditions based on a low number of measured signals. If this metamodel is not enough to fit the possible variance of the signals in the confidence interval, the procedure can fail to detect damages. If the model's uncertainty is large enough to mask the damage's effect, the methodology can also fail. Due to these reasons, the approach is appreciated for utilization in aeronautical components manufactured by composite materials since uncertainties and complexity are inherent and *sine qua non* assumptions.

Acknowledgment

The authors would like to thank the financial support provided by the Brazilian National Council for Scientific and Technological Development (CNPq) (Grant No. 306526/2019-0) and São Paulo Research Foundation (FAPESP) (Grant Nos. 2015/25676-2, 2017/15512-8, and 2019/19684-3). In addition, the authors would like to thank the anonymous reviewers and the Associate Editor for their relevant comments and valuable suggestions.

Conflict of Interest

There are no conflicts of interest.

Data Availability Statement

The data and information that support the findings of this article are freely available.¹

References

- [1] Kocijan, J., Girard, A., Banko, B., and Murray-Smith, R., 2005, "Dynamic Systems Identification With Gaussian Processes," *Math. Comput. Modell. Dyn. Syst.*, **11**(4), pp. 411–424.
- [2] Azman, K., and Kocijan, J., 2011, "Dynamical Systems Identification Using Gaussian Process Models With Incorporated Local Models," *Eng. Appl. Artif. Intell.*, **24**(2), pp. 398–408.
- [3] Worden, K., Becker, W. E., Rogers, T. J., and Cross, E. J., 2018, "On the Confidence Bounds of Gaussian Process NARX Models and Their Higher-Order Frequency Response Functions," *Mech. Syst. Signal. Process.*, **104**, pp. 188–223.
- [4] Worden, K., and Green, P., 2017, "A Machine Learning Approach to Nonlinear Modal Analysis," *Mech. Syst. Signal. Process.*, **84**, pp. 34–53.
- [5] Worden, K., and Cross, E. J., 2018, "On Switching Response Surface Models, With Applications to the Structural Health Monitoring of Bridges," *Mech. Syst. Signal. Process.*, **98**, pp. 139–156.
- [6] Villani, L. G., da Silva, S., and Cunha, A., 2019, "Damage Detection in Uncertain Nonlinear Systems Based on Stochastic Volterra Series," *Mech. Syst. Signal. Process.*, **125**(1851), pp. 288–310.
- [7] Villani, L. G., da Silva, S., Cunha, A., and Todd, M. D., 2019, "Damage Detection in An Uncertain Nonlinear Beam Based on Stochastic Volterra Series: An Experimental Application," *Mech. Syst. Signal. Process.*, **128**(10), pp. 463–478.
- [8] Rébillat, M., Hmad, O., Kadri, F., and Mechbal, N., 2017, "Peaks Over Threshold-Based Detector Design for Structural Health Monitoring: Application to Aerospace Structures," *Struct. Health Monit.*, **17**(1), pp. 91–107.
- [9] Poulimenos, A. G., and Sakellariou, J. S., 2019, "A Transmittance-Based Methodology for Damage Detection Under Uncertainty: An Application to a Set of Composite Beams With Manufacturing Variability Subject to Impact Damage and Varying Operating Conditions," *Struct. Health Monit.*, **18**(1), pp. 318–333.
- [10] Figueiredo, E., Radu, L., Worden, K., and Farrar, C. R., 2014, "A Bayesian Approach Based on a Markov-Chain Monte Carlo Method for Damage Detection Under Unknown Sources of Variability," *Eng. Struct.*, **80**(1778), pp. 1–10.
- [11] Liu, Z., Liu, X., Zhu, S.-P., Zhu, P., Liu, W., Correia, J. A., and De Jesus, A. M., 2020, "Reliability Assessment of Measurement Accuracy for Fbg Sensors Used in Structural Tests of the Wind Turbine Blades Based on Strain Transfer Laws," *Eng. Failure Anal.*, **112**(2), p. 104506.
- [12] Seventekidis, P., Giagopoulos, D., Arailopoulos, A., and Markogiannaki, O., 2020, "Structural Health Monitoring Using Deep Learning With Optimal Finite Element Model Generated Data," *Mech. Syst. Signal. Process.*, **145**(5), p. 106972.
- [13] da Silva, S., Paixão, J. A. S., Rébillat, M., and Mechbal, N., 2019, "Data-Driven Autoregressive Model Identification for Structural Health Monitoring in

¹<https://pimm.artsetmetiers.fr/>

- Anisotropic Composite Plates,” IX ECCOMAS Thematic Conference on Smart Structures and Materials - SMART 2019, N. M. Aych Benjeddou and J.-F. Deü, eds., International Centre for Numerical Methods in Engineering (CIMNE), Artes Gráficas Torres S.L, pp. 1213–1223.
- [14] Nardi, D., Lampani, L., Pasquali, M., and Gaudenzi, P., 2016, “Detection of Low-Velocity Impact-Induced Delaminations in Composite Laminates Using Auto-Regressive Models,” *Compos. Struct.*, **151**(427), pp. 108–113.
- [15] da Silva, S., 2018, “Data-driven Model Identification of Guided Wave Propagation in Composite Structures,” *J. Brazilian Soc. Mech. Sci. Eng.*, **40**(11), p. 208.
- [16] Mechbal, N., and Rebillat, M., 2017, “Damage Indexes Comparison for the Structural Health Monitoring of a Stiffened Composite Plate,” 8th ECCOMAS Thematic Conference on Smart Structures and Materials (SMART 2017), A. Güemes, A. Benjeddou, J. Rodellar, and J. Leng, eds., pp. 436–444.
- [17] Cross, E. J., Manson, G., Worden, K., and Pierce, S. G., 2012, “Features for Damage Detection With Insensitivity to Environmental and Operational Variations,” *Proc. R. Soc. A: Math., Phys. Eng. Sci.*, **468**(2148), pp. 4098–4122.
- [18] Deraemaeker, A., and Worden, K., 2018, “A Comparison of Linear Approaches to Filter Out Environmental Effects in Structural Health Monitoring,” *Mech. Syst. Signal. Process.*, **105**(2), pp. 1–15.
- [19] Rasmussen, C. E., and Williams, C. K. I., 2006, *Gaussian Processes for Machine Learning* (Massachusetts Institute of Technology), MIT Press, Cambridge, MA.
- [20] Mattos, C. L. C., Damianou, A., Barreto, G. A., and Lawrence, N. D., 2016, “Latent Autoregressive Gaussian Processes Models for Robust System Identification,” *IFAC-PapersOnLine*, **49**(7), pp. 1121–1126, [11th IFAC Symposium on Dynamics and Control of Process Systems Including Biosystems DYCOPS-CAB 2016](#).
- [21] Mujica, L. E., Gharibnezhad, F., Rodellar, J., and Todd, M., 2020, “Considering Temperature Effect on Robust Principal Component Analysis Orthogonal Distance as a Damage Detector,” *Struct. Health. Monit.*, **19**(3), pp. 781–795.
- [22] Sohn, H., Czarnecki, J. A., and Farrar, C. R., 2000, “Structural Health Monitoring Using Statistical Process Control,” *J. Struct. Eng.*, **126**(11), pp. 1356–1363.